Chinese Journal of Chemical Engineering 26 (2018) 1370–1382

Contents lists available at ScienceDirect

Chinese Journal of Chemical Engineering

journal homepage: www.elsevier.com/locate/CJChE

Article

Features of the motion of gel particles in a three-phase bubble column under foaming and non-foaming conditions☆

Gabriel Salierno [1], Mauricio Maestri [1], Stella Piovano [1], Miryan Cassanello [1,*], María Angélica Cardona [2], Daniel Hojman [2], Héctor Somacal [2,3]

[1] Laboratorio de Reactores y Sistemas para la Industria–LARSI, Dep. Industrias, FCEyN, Universidad de Buenos Aires, Int. Güiraldes 2620, C1428BGA Buenos Aires, Argentina
[2] Laboratorio de Diagnóstico por Radiaciones–LADiR, Dep. de Física Experimental, Comisión Nacional de Energía Atómica (CNEA), San Martín, Buenos Aires, Argentina
[3] Universidad de San Martín, San Martín, Buenos Aires, Argentina

ARTICLE INFO

Article history:
Received 1 December 2017
Received in revised form 27 February 2018
Accepted 12 March 2018
Available online 23 April 2018

Keywords:
Bubble columns
Solid motion
Gel beads
Foaming
Particle tracking
Mixing

ABSTRACT

Features of the motion of gel particles in a three-phase bubble column with non-foaming and foaming gas–liquid systems, determined by using experiments of radioactive particle tracking (RPT), have been compared. The tracer used is a gel particle which resembles typical immobilized biocatalyst. The tracer trajectory is analyzed to extract relevant information for design purposes. The solid velocity field, turbulence parameters, dispersion coefficients, mixing times and flow transitions are determined and compared. The presence of foam significantly affects many quantified parameters, especially within the heterogeneous flow regime. The hydrodynamic stresses are reduced in the presence of foam, especially close to the disengagement. The dispersion coefficients also decrease, and the solid mixing time is only slightly affected by the presence of foam. Gas holdup, inferred both from RPT experiments and from gamma ray scanning, is higher for foaming systems and leads to a shift in the transition gas velocity towards higher values.

1. Introduction

Bioreactor design and scale-up are still challenging issues and a detailed characterization of the phenomena that determine their behavior, especially transport processes and fluid dynamics, is crucial for establishing scaling rules [1,2]. The fate of cell aggregates or immobilized biocatalysts while promoting reaction in a biochemical process is decisive for selecting design variables and operating conditions [3,4]. In this sense, it is important to map the zones of high degree of turbulence to prevent hydrodynamic stress [5].

In the last decades, applications of immobilized enzymes or cells in multiphase reactors have progressively increased. Three-phase bubble columns or fluidized-bed reactors have been frequently chosen due to their advantages, like the minimized stagnant areas and the possibility of solid removal without stopping the operation [6]. Calcium alginate is a gel traditionally used for fermentations to immobilize enzymes and living organisms by retention. Its potential use as support for inorganic catalysts employed in wastewater treatment has also been proposed [7]. Hence, examining the motion of flexible gel particles, representing immobilized biocatalysts or solid aggregates, in a three-phase bubble column will contribute to defining design strategies and operation conditions in these systems. Even if flexible gel particles are commonly found in many processes, particularly in bioprocesses where immobilized or aggregated cells are suspended, the motion of these particles has been scarcely examined. Moreover, comparing their motion in foaming and non-foaming conditions can shed light on the beneficial and/or detrimental effects of foam.

Foaming systems frequently appear in the chemical and biochemical industries, and in wastewater treatment processes. The liquid in several processes may contain surfactants inhibiting bubble coalescence and promoting foam formation [8]. Surfactants generally increase the gas holdup, stabilize the homogeneous regime and modify the bubble shapes and size distributions [9]. Biochemical processes recurrently encounters foaming systems, arising from the surface-active characteristics of many bio-based products [10]. Foam is generally not desirable but it may be difficult to eliminate with antifoaming agents. When removed from the surface by mechanical shafts, it may still exist in the broth bulk. Moreover, for bio-surfactants and lipopeptide production, or for removing contaminants with low water solubility, a foam out-stream has been proposed to improve the process [11–15].

The solid motion within a turbulent media is best examined with non-invasive methods; radioactive techniques proved to be appropriate for extracting thorough information in different multiphase systems. Particularly, radioactive particle tracking (RPT) is an advanced

☆ Supported by the FONCyT (PICT2014-0704), CONICET (PIP1122015-0100902CO), and Universidad de Buenos Aires (UBACyT 20020130100544BA).
* Corresponding author.
E-mail addresses: miryan@di.fcen.uba.ar (M. Cassanello), hojman@tandar.cnea.gov.ar (D. Hojman), somacal@tandar.cnea.gov.ar (H. Somacal).

https://doi.org/10.1016/j.cjche.2018.03.026
1004-9541/

tomographic method that allows recovering the path of a tracer freely moving in a 3D media for prolonged periods of time. RPT has been successfully applied to study two- and three-phase bubble columns intended for fermentation purposes [16].

The motion of gel flexible particles, which typically represent biocatalysts immobilized by retention, has been examined and recently reported by the authors only under foaming conditions [17]. However, the information of gel particles motion under non-foaming conditions, which represent many typical situations, is lacking. Hence, the purpose of this work is to study the motion of a gel particle with the same size, density, wettability and texture of the other particles, freely moving in a three-phase bubble column. The actual path and features extracted from the long tracer trajectory are analyzed comparatively for the gas–liquid system with and without foam. The influence of the gas velocity on the solid velocity field, solid distribution and turbulence parameters is examined within a range covering the bubbling and the churn turbulent flow regimes, under foaming and non-foaming conditions. The results give further insights of flexible gel particles dynamics and highlight the effect of foam.

2. Experimental

The three-phase bubble column used for the experiments had 1.2 m height and 0.1 m internal diameter. The model liquids used were a 0.5 $mol \cdot L^{-1}$ $CaCl_2$ aqueous solution, and the same solution with added benzalkonium chloride (0.1×10^{-6}) to promote foaming. The solid particles were calcium alginate beads of 5 mm mean diameter. The gel particles were prepared by extrusion dripping of a 1.5wt% sodium alginate aqueous solution received in a 0.5 $mol \cdot L^{-1}$ $CaCl_2$ solution. A peristaltic pump that ends in a needle was used to produce the drops of sodium alginate, which formed the calcium alginate beads by ion exchange afterwards [18]. The gas phase was compressed air, with dust and oil filters. It was introduced into the column through a spider type perforated plate distributor with 32 holes of 1 mm diameter (0.32% of the column cross-section), located in the base of the column ($z = 0$). Liquid and solid were in batch, and the gas velocities ranged from 0.021 to 0.095 $m \cdot s^{-1}$, for exploring the bubbling, transition and the incipient churn turbulent flow regimes. Photographs of the bubble column with both test liquids, operating at similar conditions are illustrated in Fig. 1a (no foaming) and 1b (foaming), for comparison.

The tracers used to track the solid phase were prepared to have the same size and density, and also the texture and wettability of the suspended gel particles. Texture and wettability features are important because they strongly affect the adherence of gas bubbles on the solid surface. The tracers were prepared by incorporating tiny gold nuggets of around 0.05 mg into calcium alginate spheres. Since the gel particles shrink when they are perforated or left out of liquid, it was not possible to introduce the gold nugget inside an already prepared gel bead. So, they were first introduced within perforated high density polyethylene (HDPE) beads of 1 mm, to ease their manipulation. The HDPE beads containing the gold nuggets were sent to the RA1 nuclear reactor of the National Commission of Atomic Energy (CNEA) of Argentina for activation by neutron bombardment. Gold 197 has a high neutron capture cross section [19], which allows using very small nuggets and a moderate exposure to neutron bombardment to obtain appropriate activities for performing RPT experiments. After neutron bombardment, the tracer used contained ^{198}Au ($t_{1/2} = 2.7$ d, Epeak $= 412$ keV) and an activity of around 50 μCi. It was also simpler and safer to handle the 1 mm plastic beads than the gold nuggets, since the gold nugget diameters were generally less than 0.2 mm. Afterwards, the gel particle was prepared in a mold designed for producing first a half sphere of calcium alginate, then incorporating the plastic bead containing the already activated gold nugget inside, and finally casting the other semisphere on top in the same mold. A scheme of the mold is shown in Fig. 1c. The photograph of one prepared tracer is shown in Fig. 1d.

The "instantaneous" tracer positions were reconstructed considering the photon counts simultaneously detected by the scintillators every 30 ms. For the reconstruction, a calibration stage was performed by measuring the counts while locating the tracer at known positions within the three-phase emulsion. With the signal distribution, the tracer intensity, the media attenuation and the dead time of the detector system were fitted for each detector to represent their response to

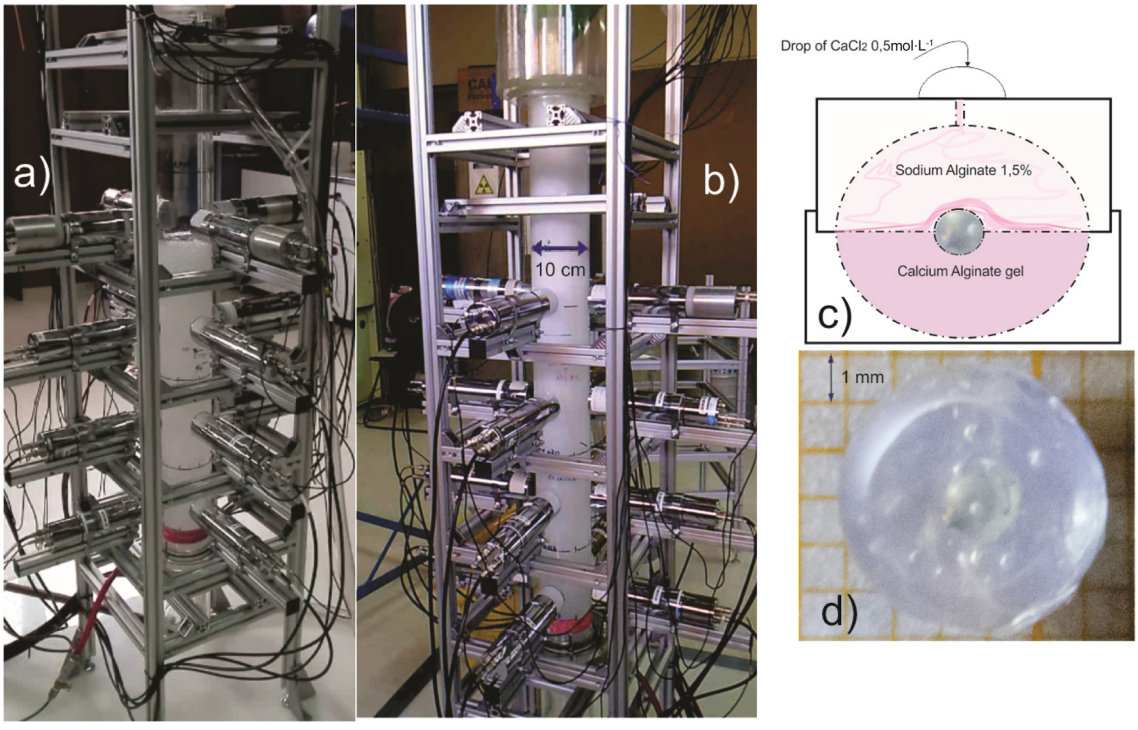

Fig. 1. Three-phase bubble column with a non-foaming (a) or foaming (b) gas–liquid system; (c) scheme of the mold used for preparing the radioactive tracer, (d) a prepared radioactive tracer.

radiation. Then, a database of correspondence between positions within the reactor and signal distribution was created and used to get the positions of a tracer in free motion within the emulsion. Further details of the reconstruction procedure can be found elsewhere [20,21].

The gas holdup was estimated by two independent methods to diagnose the gas velocity leading to the transition between homogeneous and heterogeneous flow regimes. One way relies on measuring the bed expansion to get the three-phase emulsion total volume. Then, as the solid and liquid are in batch, the gas holdup is obtained considering the bed expansion and the volume of the dense phases at rest. Bed expansion can be identified by visual inspection. However, it is difficult to see the liquid height when the solid has the same color as the liquid, and even worse if there is foam. Moreover, defining the liquid level by visual inspection is generally subjective. RPT experiments provides an objective way of getting the bed expansion, since the tracer explores the whole three-phase emulsion as it is totally similar to the other particles in the bed. The tracer travels in the disengagement axial coordinate many times during the long tracking observation period. Therefore, one can observe all the axial positions of the tracer and estimate the bed expansion from the highest values attained. Since the particle can be sometimes attached to a bubble, it may occasionally jump over the disengagement; hence, it is advisable to take an average of many positions to avoid overestimation of the upper bed limit. We have decided to compute the mean of the 100 highest positions, since with this number, the tracer almost covers the whole section, and represents a good statistics, without underestimating the limit. Generally the means of 50 to 200 highest positions do not vary significantly.

Another way of objectively estimating gas holdups is from gamma ray densitometry experiments. Densitometry is used for two-phase systems (*e.g.*, gas–liquid). For three-phase, two sources of different energies would be required, in principle. However, in this case, the solid phase has almost the same attenuation as the liquid phase because the gel particles have density and composition similar to the liquid. Therefore, one can assume a pseudo liquid–solid phase of a unique attenuation coefficient, significantly different from the gas attenuation. Hence, with gamma scanning, the chordal gas holdup can be obtained by measuring the absorbed intensity of an external source under the examined experimental conditions, for the empty and the flooded column (see Chapter 1 of [21] for further details).

The chordal gas holdup was determined in this work by gamma ray densitometry experiments at ten column heights using an external 2 mCi ^{242}Am source under the experimental conditions used for RPT experiments. Naturally, while performing the scanning experiments, the tracer used for RPT was removed from the column. The attenuation of the external radioactive source was measured at different column heights locating the detectors axially aligned beside the column, and manually moving the external source. The attenuation of the empty and the flooded column were measured for the same heights. The chordal gas holdup was then determined as:

$$\varepsilon_G = \frac{\ln\left(\frac{I_{3\varphi}}{I_F}\right)}{\ln\left(\frac{I_G}{I_F}\right)} \tag{1}$$

where I_G is the intensity measured by the detector after crossing the column when the column is empty, I_F, the same when the column is flooded and $I_{3\varphi}$ is the intensity after crossing the column for an operating condition.

3. Results

3.1. Solid velocity fields

Radioactive particle tracking experiments provide the actual position of a tracer, which perfectly mimics the other particles in the bed, every 30 ms for several hours. From this tracer positions, the instantaneous velocities of the tracer are calculated considering the linear estimation of 3 consecutive positions. To get the velocity field, the examined vessel is discretized into voxels in 3D and the instantaneous velocities calculated from three consecutive positions are assigned to the voxel that contains the middle position of the tracer for that instant. Then, assuming the hypothesis of ergodicity (*i.e.*, one particle observed at different times represents other particles), ensemble average of particle velocities can be calculated for all the regions within the column (for further details, see Chapter 11 of [21]). Projections of the flow field of the non-foaming system are shown in Figs. 2 and 3 for various operating conditions. These projections can be compared to those shown in [17] that correspond to the same conditions with the foaming gas–liquid system.

Under non-foaming conditions, the radial-axial projection indicates an ascending motion in the column center and descending close to the wall. An inversion region is apparent at a dimensionless radius of $r/R \sim 0.7$. This behavior is similar to those found for particles denser than the liquid phase (*i.e.*, glass beads, PVC extrudates [22]) and for the liquid in bubble columns [23]. In this system, the particles density is very close to the liquid density; hence, the behavior is likely similar to the one found for neutrally buoyant tracers, intended for tracking the liquid phase. Comparing with the velocity fields obtained in the foaming system [17], the ascending velocities in the column center are more definite and larger in magnitude for experiments in the heterogeneous flow regime.

Fig. 3 illustrates an axially averaged projection of the velocity field onto the column cross section for the non-foaming system. There is no clear rotational motion and the velocity fields resemble results obtained for gas–liquid and three-phase bubble columns with denser particles [22,23]. Compared to the foaming system [17], there is no inwards flow close to the column wall, remarking that the foam is responsible for the negative radial velocities found in foaming gas–liquid systems. Thus, the foam likely occasions a hindrance effect for the solid close to the wall.

3.2. Turbulent kinetic energy distribution

Exposure of biocatalysts to hydrodynamic stress caused by high level of turbulence is a major concern in many fermentative processes, particularly for sensitive cells [24–26]. In bubble columns and air-lift reactors, the region where the highest damage is supposed to occur is close to the disengagement [27]. Bubble bursts have been generally considered as responsible for the decrease in the number of viable cells as gas velocity is increased. Then, shear protective agents used for mitigating the stress are frequently surfactants that promote foam formation, thus decreasing the effect of bubbles bursts in their exit from the three-phase emulsion.

The normal and shear stresses to which the biocatalysts are exposed at different locations in the column can be quantified from RPT experiments [17]. The Reynolds stress tensor, calculated from the components of the fluctuating velocities for any region within the column allows estimating the stress encountered by the cells. The tensor is determined as expressed in Eq. (2), where r, θ and z are the radial, azimuthal and axial coordinates and u'_j indicates the "j" component of the fluctuating velocity.

$$\frac{\tau}{\delta} = \begin{pmatrix} \overline{u'_r u'_r} & \overline{u'_r u'_\theta} & \overline{u'_r u'_z} \\ \overline{u'_\theta u'_r} & \overline{u'_\theta u'_\theta} & \overline{u'_\theta u'_z} \\ \overline{u'_z u'_r} & \overline{u'_z u'_\theta} & \overline{u'_z u'_z} \end{pmatrix} \tag{2}$$

The sum of normal stresses in the three directions (*i.e.*, the tensor trace) is known as the turbulence kinetic energy (TKE). The shear stresses are the cross products of the components, and they are generally quite lower than the TKE [17,21]. In addition, the axial normal stress largely

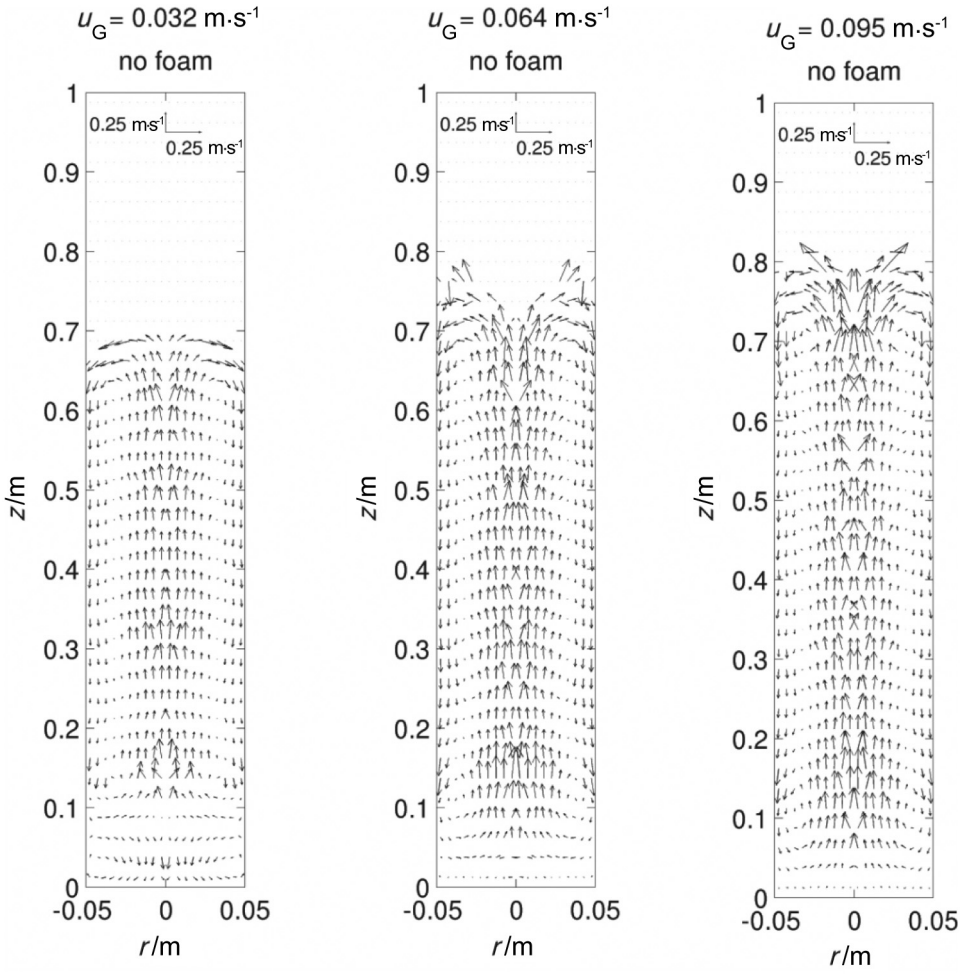

Fig. 2. Axial–radial velocity fields (azimuthally averaged) for gas velocities representative of the bubbling, transition and churn-turbulent flow regimes in the non-foaming system.

overcomes the normal stresses in the other directions for bubble columns of high aspect ratios. Therefore, TKE can provide an indication of the largest hydrodynamic environmental effect on the moving biocatalysts.

Three regions in a bubble column have been identified where cell-bubbles interaction can cause cells damage and eventually death: at the sparger where the bubbles are formed, in the bulk region where the bubbles rise fast and at the disengagement where the bubbles exit the three-phase emulsion [27]. Normally the entrance and disengagement regions have been considered to exhibit the worse conditions. Sectional distribution of TKE around three columns heights (entrance, mid-height and exit) are shown in Figs. 4 and 5 for gas velocities representative of the homogeneous and heterogeneous flow regimes (see Section 3.5 for flow transition).

TKE values are significantly lower within the homogeneous flow regime all over the column. Close to the disengagement region TKE is lower in the homogeneous than in the heterogeneous regime since bubbles are generally small and dispersed; hence, they do not burst strongly when they exit from the three phase emulsion. For low gas velocities the values are only slightly dependent on column region. Comparing foaming and non-foaming conditions, differences are mild,

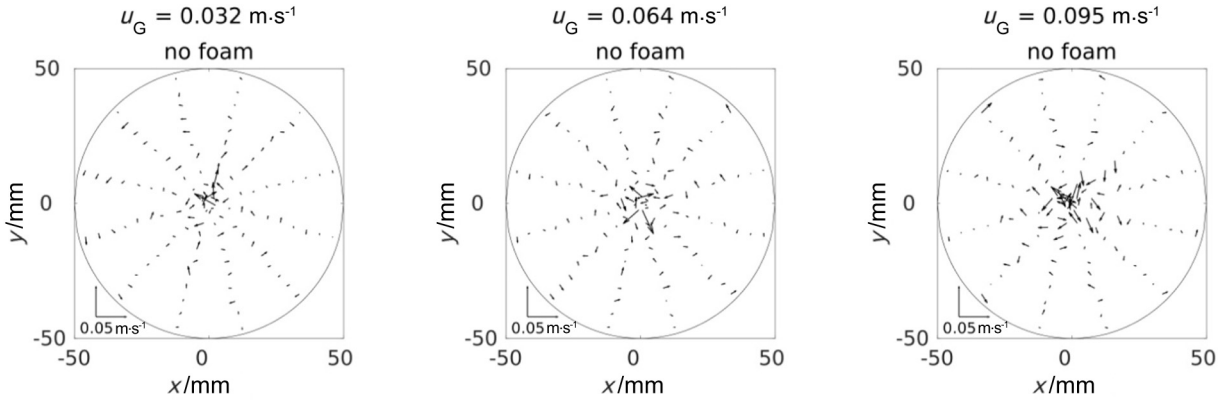

Fig. 3. Velocity fields (axially averaged) on the transversal plane for the non-foaming system, for gas velocities representative of the bubbling, transition and churn-turbulent flow regimes.

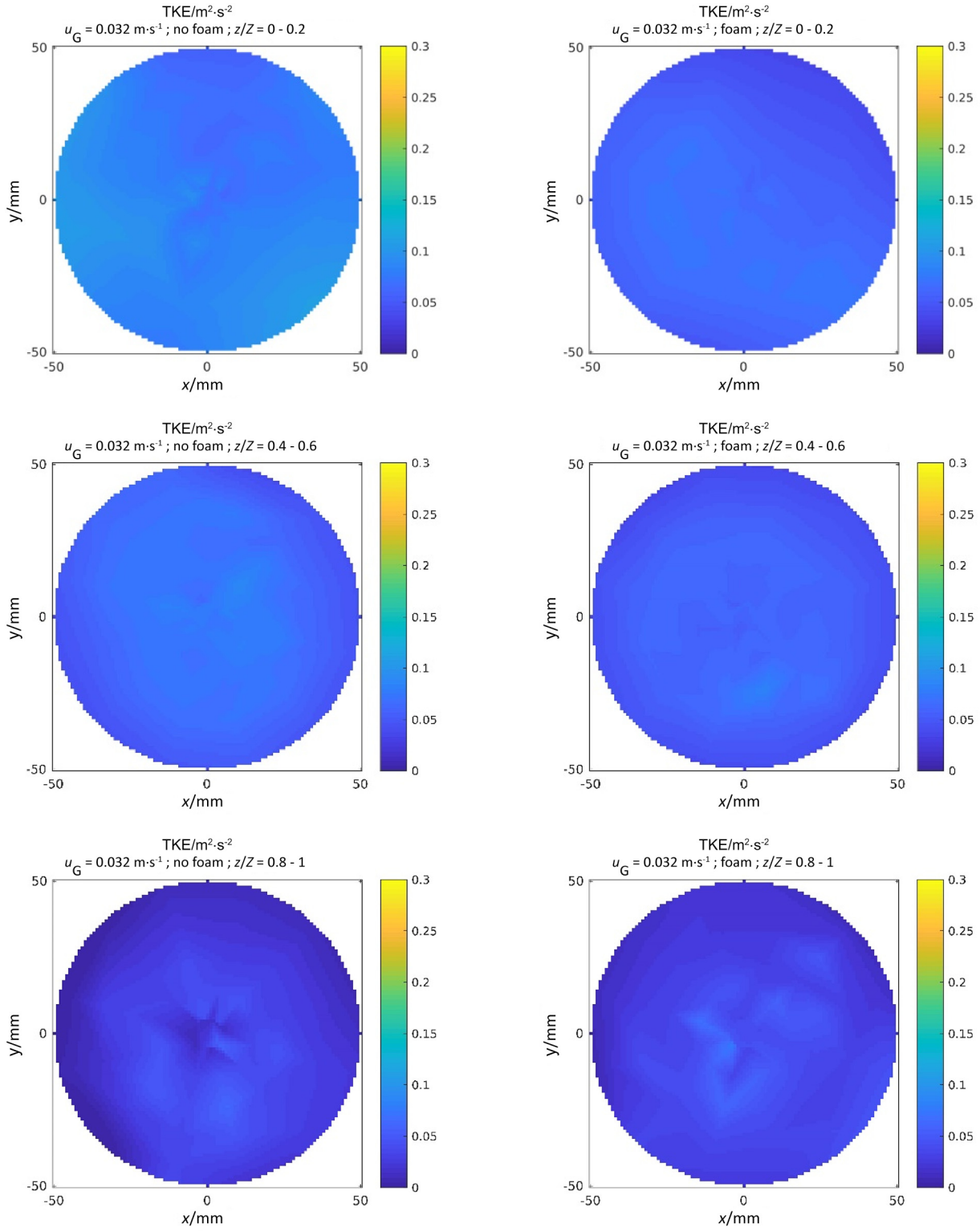

Fig. 4. Maps of the TKE for a gas velocity in the homogeneous flow regime, for non-foaming (left) and foaming (right) systems, at different axial regions.

although values under non-foaming conditions can be larger for given locations around the column center. For high gas velocities, the distribution is more heterogeneous, particularly close to the disengagement. Moreover, differences between foaming and non-foaming conditions become apparent in the majority of the column, especially in the column top, where the bubbles burst effect is expected to be very important.

The radial profiles of TKE calculated for the entrance and exit regions for foaming and non-foaming systems at different gas velocities are illustrated in Figs. 6 and 7. Experiments pertaining to the homogeneous and heterogeneous flow regimes, as determined form a break in the gas holdup *vs.* gas velocity curve (see Section 3.5), are shown for comparison.

TKE profiles are almost uniform in the radial direction, descending only slightly close to the column walls for certain conditions. As observed in the maps, the flow regime markedly affects the TKE for non-foaming systems in the upper region (Fig. 6) close to the bubbles

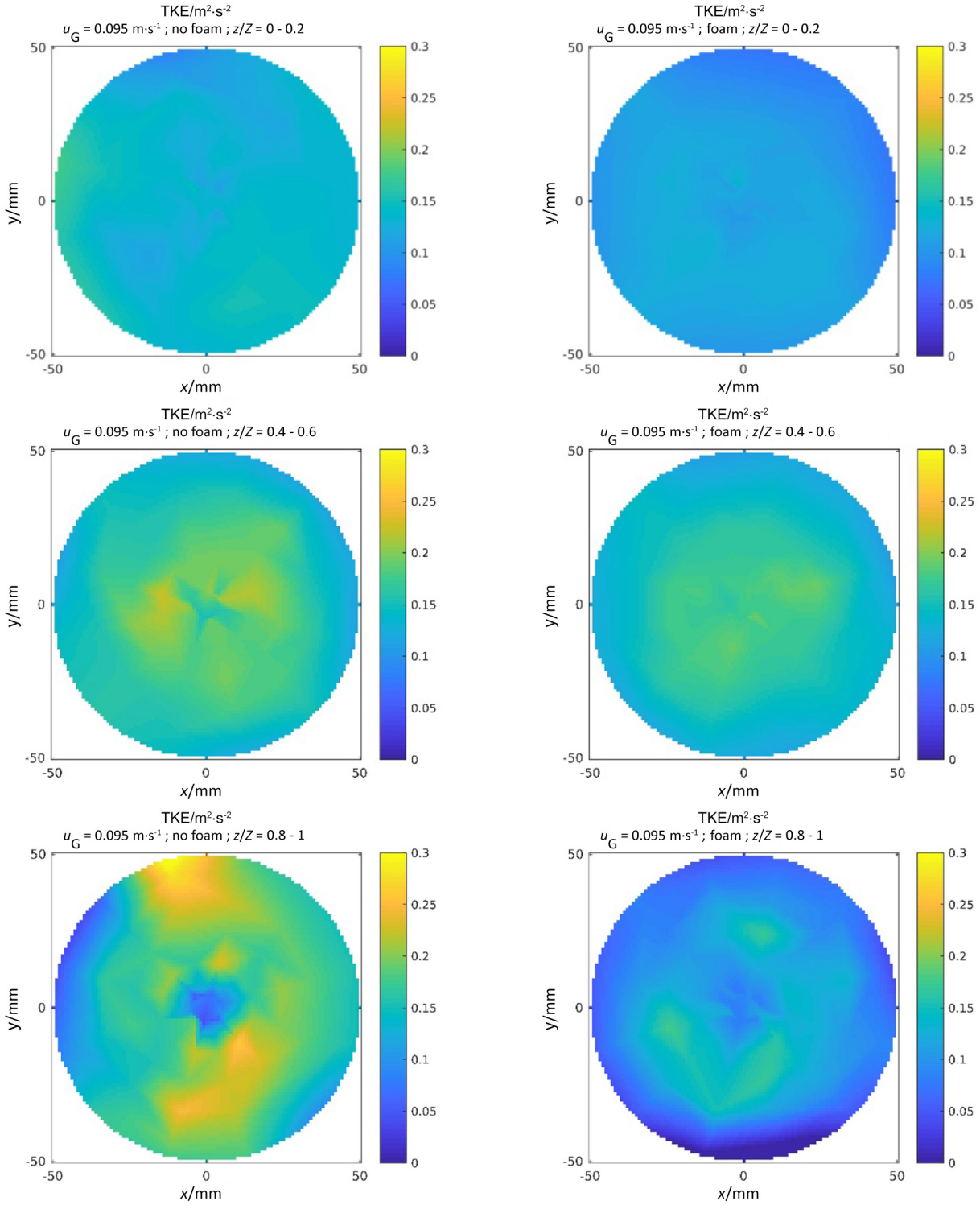

Fig. 5. Maps of the TKE for a gas velocity in the heterogeneous flow regime for non-foaming (left) and foaming (right) systems, at different axial regions.

bursts, where the values strongly increase with the gas velocity after the flow transition. The sharp increase associated with a change in flow regime for non-foaming systems has been observed for bubble columns of large diameter [23]. In contrast with this behavior, for foaming systems, the gas velocity has less effect on the TKE level, supporting the shear protective action of surfactants for mitigating the hydrodynamic stress close to the disengagement region.

Near the sparger there is apparently no significant influence of the flow regime, and the foam has almost negligible effect in that region; differences between the results for foaming and non-foaming systems are low (Fig. 7). As observed also in the maps, the protective action of surfactants is low in the entrance region, where the stress is likely to be related to the energy dissipated by the gas jets.

It has been argued that, even if the cells are damaged within regions of high level of turbulence, the risk is also related to the time during which the cells effectively remain in those regions [25]. Although bubble bursts are very harsh for isolated cells, if cells are immobilized or form large aggregates, those are less frequently driven towards the disengagement

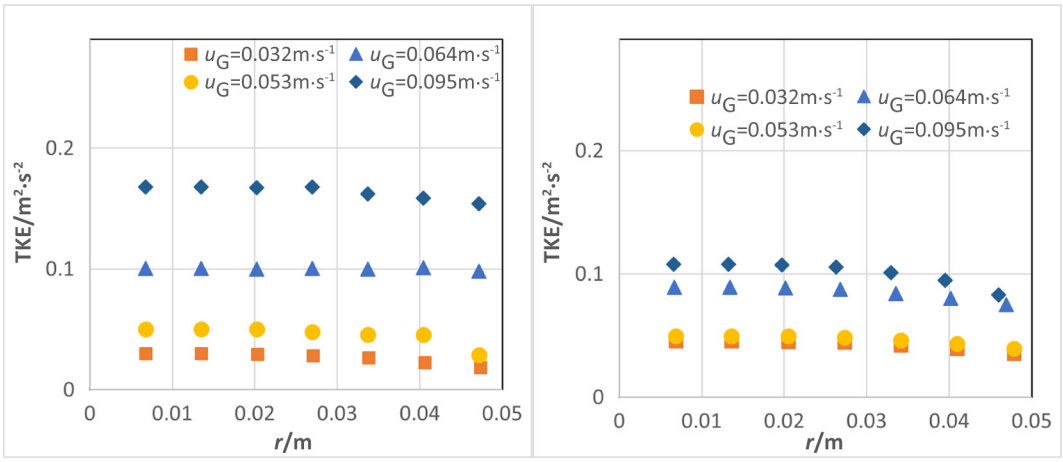

Fig. 6. Radial profiles of the TKE in the upper region of the column for non-foaming (left) and foaming (right) systems, for various operation conditions. Average in the range $z/Z = 0.85–1.0$.

region, and the damage risk is consequently reduced [17]. This is not the case in the entrance region, where the large aggregates remain longer periods both for foaming and non-foaming systems.

Zhong and Yuan [27] have studied the influence of the sparger nozzle size on plant cells viability, comparing nozzles diameters of 1, 1.5 and 2 mm. These authors found that the bigger the nozzle diameter, the less cell damage is apparent, as judged from the viable cells growth, pointing to a strong influence of the gas injection onto the hydrodynamic stress suffered by the biocatalysts.

From the fluctuating velocities, calculated as the instantaneous minus the local mean velocity of the assigned voxel, the turbulent kinetic energy can be estimated for all the column regions, as expressed in Eq. (2). Fig. 8 shows the frequency distribution of TKE for representative conditions. Note the remarkable damping effect of foam on the TKE, inferred from the comparison of the distributions obtained for non-foaming and foaming systems. Whatever the gas velocity is, the maximum TKE in the distribution of non-foaming systems is more than twice the value calculated for the foaming system under similar conditions. For non-foaming systems, the distributions are broader than under foaming conditions, remarking the larger heterogeneity of the systems probably related to the presence of large bubbles.

The mode or the mean of the distribution may be considered as a reasonable estimation of the average specific hydrodynamic stress faced by the cells. Taking into account that the liquid and the solid density are very close to the water density, the values in pressure units can be calculated. For non-foaming systems, the mean values go from around 60 Pa for low gas velocities to 120 Pa for the highest gas velocity examined. Comparatively, for foaming systems, the mean values go from around 30 Pa for low gas velocities up to 50 Pa for the highest gas velocity. The differences between foaming and non-foaming conditions depend slightly on gas velocity within the homogeneous flow regime, and increase significantly after the transition.

3.3. Solid dispersion coefficients

The radial and axial solid dispersion coefficients characterizing the particles motion can also be obtained from RPT experiments. The time dependence of the mean square displacements of particles starting their trajectory from a given region can be reconstructed from the long tracer trajectory determined by RPT. Manifolds of particles trajectories starting from different column regions are obtained by considering that each time the tracer crosses a given location, it represents a different particle starting its motion from the same point. To avoid correlation, selected extracts of the trajectory should be properly separated in time among them. For example, 15 trajectories of one such manifold have been represented in Fig. 9. The variance of the trajectories gives the mean square displacement of the particles starting their path at an initial position, $\overline{x_0}$, close to the column center in the example.

The mean square displacement has a linear relationship with the elapsed time after an initial period of correlation. Then, by using the Stokes-Einstein relation, the dispersion coefficient can be calculated from the linear scaling region between the mean square displacements

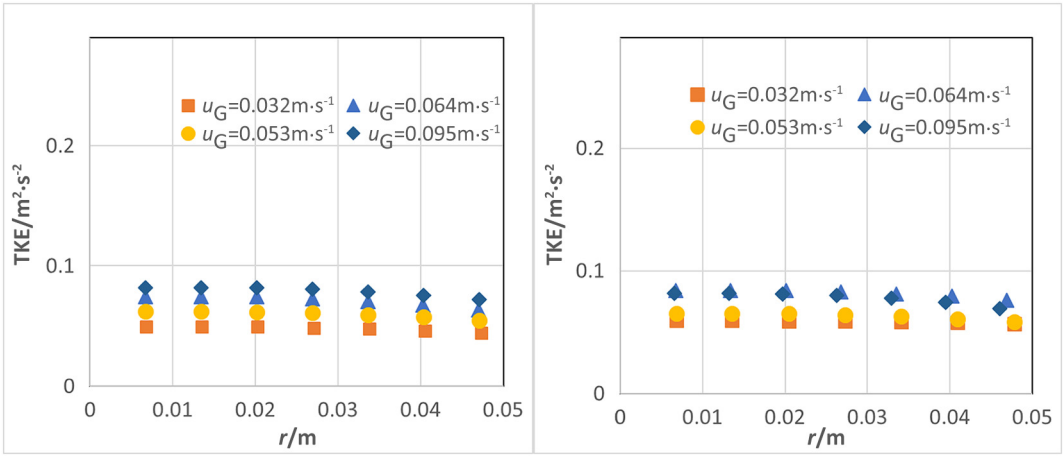

Fig. 7. Radial profiles of the TKE in the entrance region of the column for non-foaming (left) and foaming (right) systems, for various operation conditions. Average in the range $z/Z = 0–0.15$.

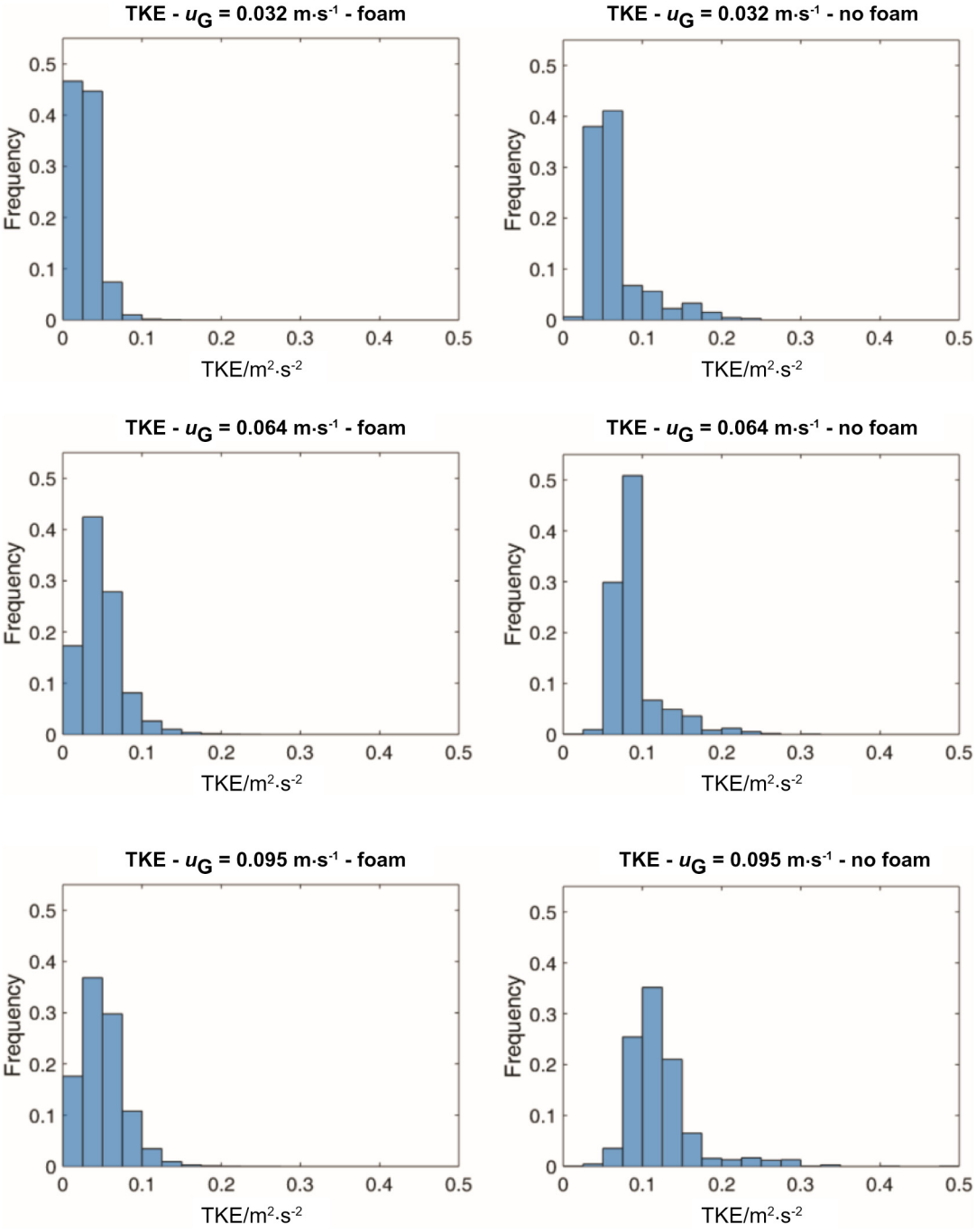

Fig. 8. Histograms of time-averaged turbulent kinetic energy for conditions representative of the bubbling, transition and the churn-turbulent flow regimes for foaming (left) and non-foaming (right) systems.

and the elapsed time, τ, between the actual time and the instant when the trajectories started their path from the considered position (Fig. 9, right). The linear region is generally apparent between 0.3–0.5 s and 1–1.5 s after the time considered as initial time. Eq. (3) provides the relation between the dispersion coefficient, D, and the mean square displacements of trajectories, valid within the linear scaling region:

$$D = \frac{1}{2\tau}\left\langle \xi^2 \right\rangle_{(\tau)} = \frac{1}{2\tau}\sum_i \left(\left|\overline{x}_{i(\tau)} - \overline{x_o}\right|\right)^2 \quad (3)$$

where $\langle \xi^2 \rangle_{(\tau)}$ is the variance of the trajectories with starting point $\overline{x_0}$ at the time $\tau = (t - t_0)$, t_0 is the starting time of each *i-th* trajectory of the manifold.

Solid dispersion coefficients calculated from displacements in the radial and axial directions are shown in Fig. 10 for the foaming and non-foaming systems. Shown values are obtained as the mean of dispersion coefficients determined from 15 axial, 3 radial and 6 azimuthal (270 in total) initial positions within the column. Selected initial positions form manifolds of at least 100 extracted trajectories to ensure good statistics. Differences among calculated values do not overcome 10%, as indicated in the error bars shown in Fig. 10. Even if a positive influence of the gas velocity is apparent for both systems, the damping effect of the foam on the effect of gas velocity is noteworthy both for the radial and axial directions. Solid dispersion in non-foaming systems is significantly higher than in foaming system, particularly for gas velocities leading to the heterogeneous flow regime.

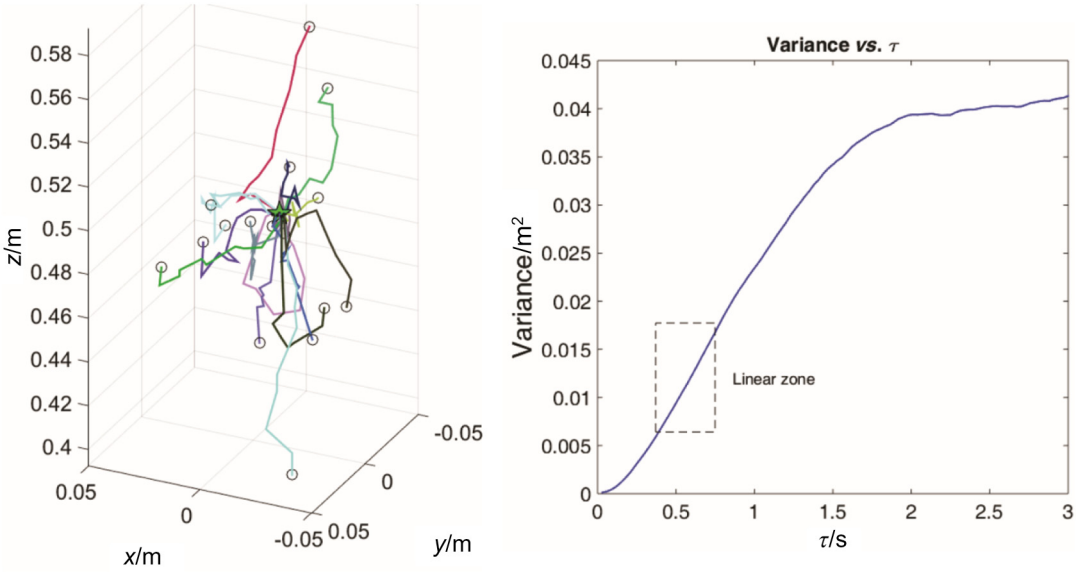

Fig. 9. Representative 15 trajectories starting from the same spatial voxel (left) pertaining to a manifold used for calculating the dispersion coefficients. Variance of the axial component of all the trajectories starting from the same point, as a function of the elapsed time (right).

3.4. Mixing times

Solid mixing time is another feature of the solid motion that can be estimated from RPT experiments. The time required for a group of particles to attain the asymptotic solid distribution after being introduced at a giving location would represent an estimator of the solid mixing time. To judge if the asymptotic distribution has been reached, one can rely on the notion of entropy [28] and use the manifolds obtained as described in the previous section. To quantify the entropy, the column is discretized in bins (30 in the axial, 5 in the radial and 8 in the azimuthal directions). As in the case of dispersion coefficients, bigger voxels than those used for calculating the velocity fields and the TKE spectrum are used to have better statistics, at least 100 trajectories in the considered manifold.

The entropy is calculated by the definition used in the theory of information [29], and normalized by the entropy of a uniform distribution, as expressed by:

$$\Omega(t) = -\frac{\sum_{i=1}^{N}\left[p_{i(t)}\ \ln\left(p_{i(t)}\right)\right]}{\ln(N)} \tag{4}$$

where N is the number of bins into which the space is discretized, $p_{i(t)}$ is the probability of the i-th bin at time t. The probability is calculated as the number of events in the i-th bin divided by the total number of events considered at time zero in the starting point. The number of events is the number of extracts of trajectories forming the considered manifold.

The calculated probabilities increase from zero (at the initial time, all the "particles" located in a given bin, from which all the trajectories start) to an asymptotic maximum value, which depends on the stabilized solid distribution. If normalized by the maximum entropy (*i.e.*, uniform distribution, the same fraction of particles for every bin), the asymptotic value would be lower than or equal to 1. The maximum entropy is not attained because the solid holdup profile is slightly higher in the lower region of the column; hence, the uniform distribution is never reached. The asymptotic value for the normalized entropy should be independent of the injection point; it should only depend on the stabilized solid distribution. It can be calculated from the distribution of all the tracer positions for the considered vessel discretization. Attained values are generally between 0.80 and 0.95. The mixing time is taken as the time required for attaining the asymptotic value of the normalized entropy. For diagnosing that the asymptote has been reached from a given injection point, the difference between the normalized entropy calculated from the manifold of "injected" trajectories and the asymptote calculated from the solid distribution is considered (see Fig. 11). Fig. 11 shows the time variation of the normalized entropy for two representative injection

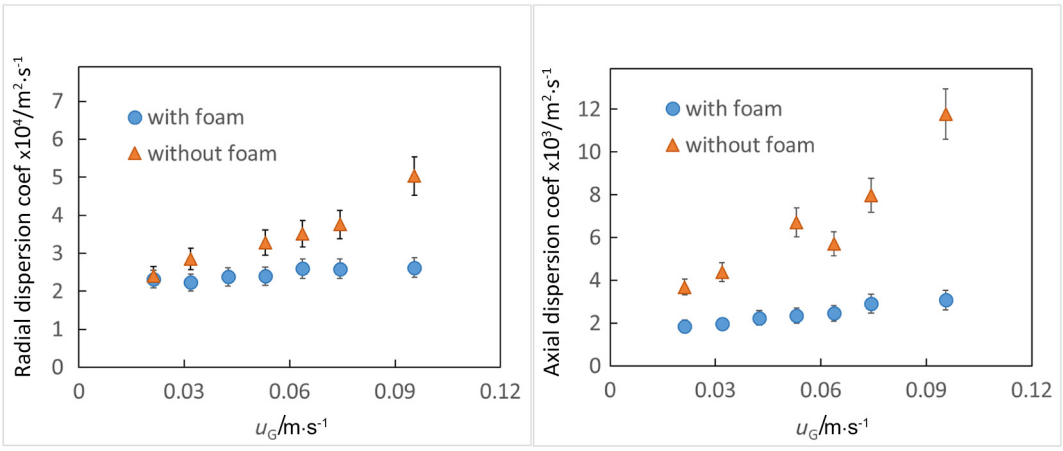

Fig. 10. Comparison of solid dispersion coefficients in the radial direction (left) and axial direction (right) as a function of gas velocity.

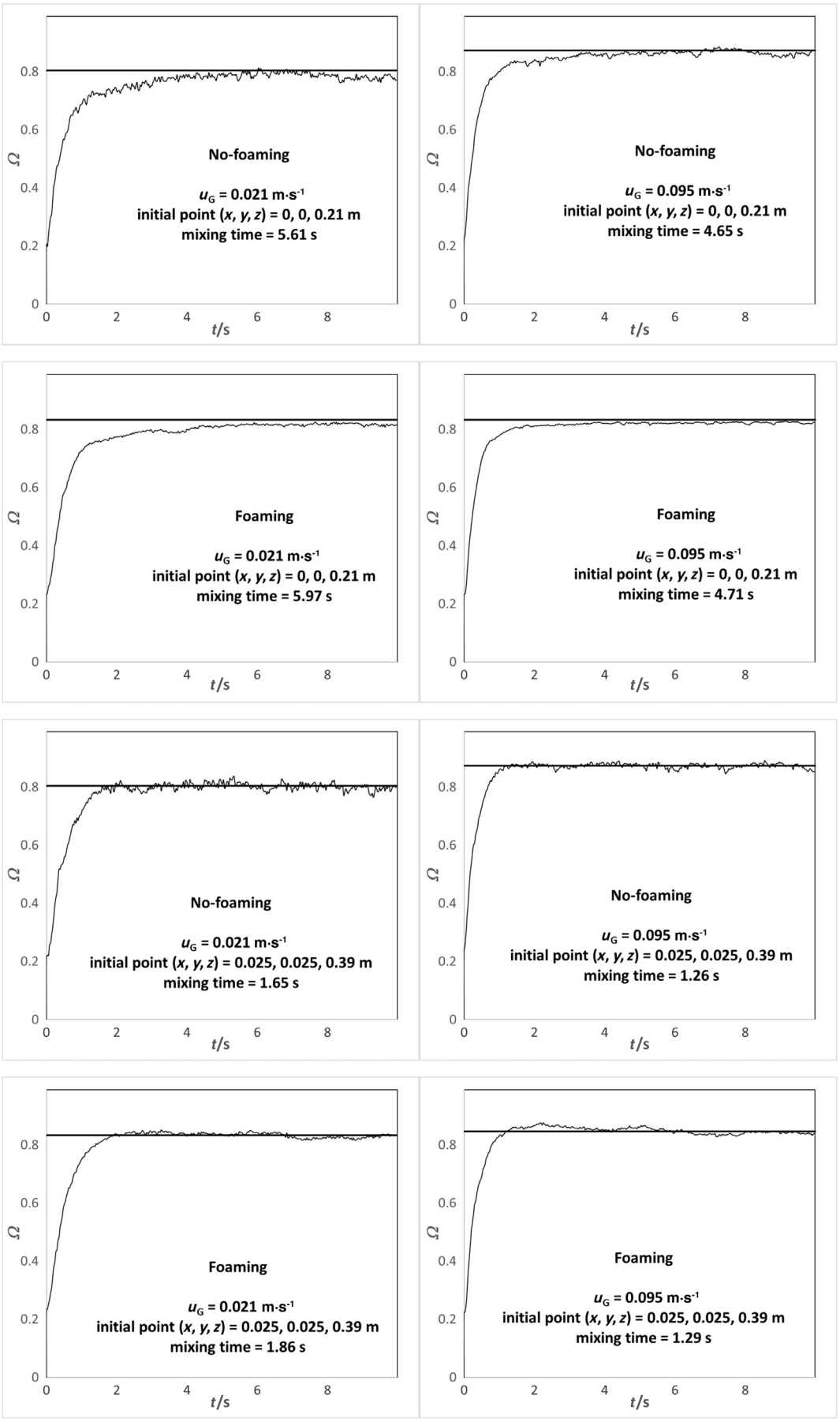

Fig. 11. Time evolution of the normalized entropy for non-foaming and foaming systems. Gas velocities and starting axial positions are indicated in the legend.

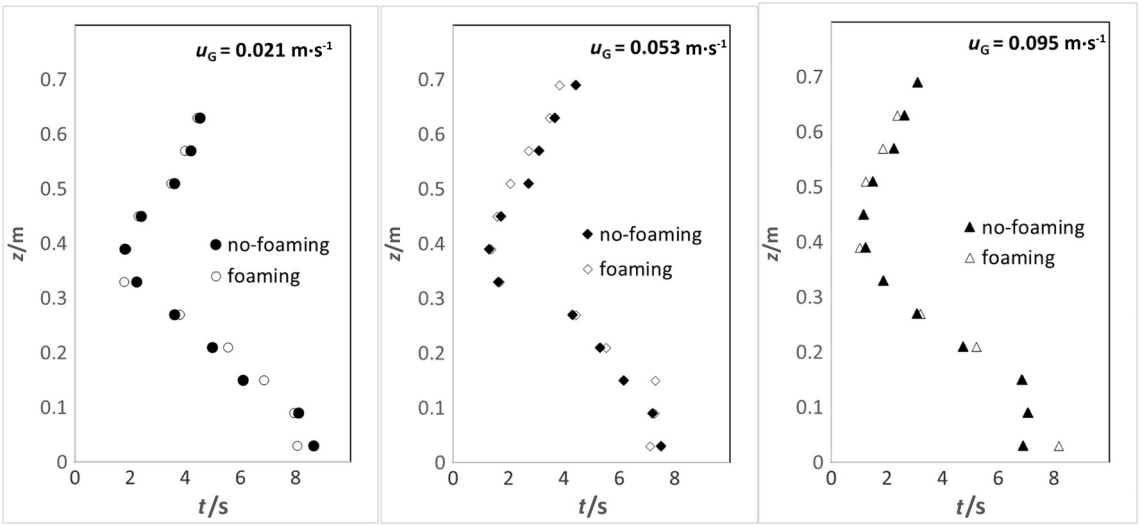

Fig. 12. Comparison of solid mixing times axial profiles for conditions representative of the bubbling and the churn-turbulent flow regimes.

positions and conditions under the homogeneous and the heterogeneous flow regimes, for foaming and non-foaming systems. The mixing time and the asymptotic value are indicated in the figure.

For bubble columns with high aspect ratio, the total mixing time does not differ significantly from the axial mixing time because the radial limits are reached quite before the axial limits. Hence, the solid axial mixing times are determined for different column heights, by considering different starting locations and taking the average of all the starting locations with the same axial coordinate. Fig. 12 shows the time required to reach the stabilized solid axial distribution while starting from different column heights, for representative experimental conditions for the foaming and non-foaming systems.

Mixing times are similar for both systems. They are likely more related to the gross circulation patterns observed in the velocity fields than to the dispersion coefficients. When the "injection" positions are below $Z/D \cong 2$, mixing times are longer than from all other starting axial locations. From this axial region, which is below the position where the two macroscopic vortical structures (observed in the velocity fields) merge, the time required for attaining the asymptotic solid distribution increases. Hence, the particles starting their path within the lower vortical structure need longer time to reach the upper region of the column. Above $Z/D \cong 2$, the mixing times are low probably because the particles are likely to travel upwards or downwards, while from other regions, they generally have a preferential direction. As the axial initial position increases and approaches the upper bound, the mixing time increases again.

3.5. Gas holdup and flow regime transition

The chordal gas holdups determined by gamma ray densitometry at ten column heights for the foaming and non-foaming systems are shown in Fig. 13. There is a slight increase in chordal gas holdup up to z around 0.45 m in both systems. Then, as the disengagement region

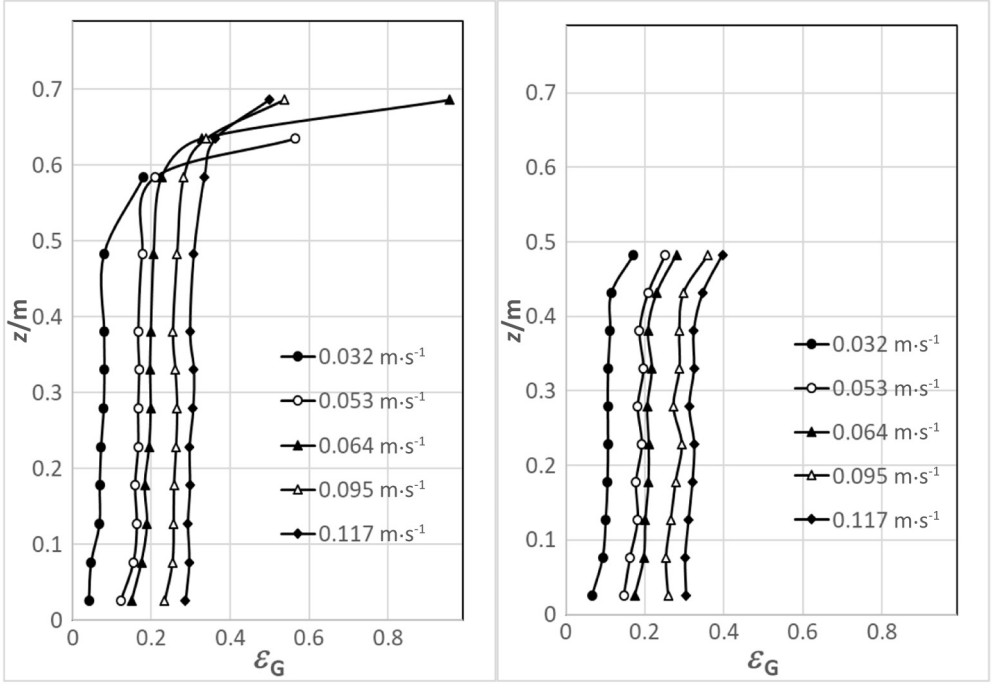

Fig. 13. Axial profiles of the gas chordal holdup determined by gamma ray scanning for non-foaming (left) and foaming (right) systems.

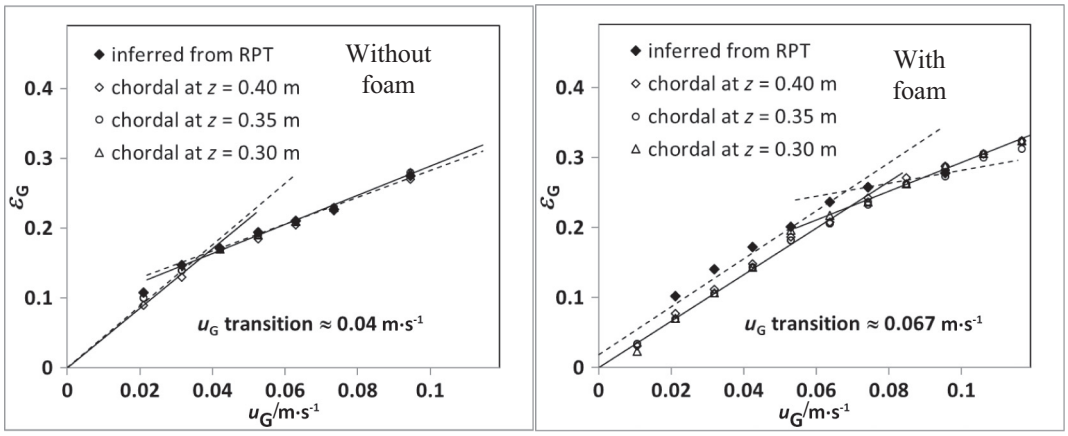

Fig. 14. Influence of the gas velocity on the gas holdup inferred from RPT or on the chordal gas holdup determined by gamma ray densitometry. The gas velocity at the flow regime transition is determined from the trend break.

is approached, the chordal gas holdup increases sharply, as observed in the case of the non-foaming system. The foaming system was examined only in the lower part of the column. Comparing both systems, it arises that the gas holdup is larger in the foaming system for all the axial locations and under all the examined experimental conditions.

The three-phase emulsion expansion can be inferred from RPT experiments from an average of the highest tracer positions within the prolonged track period. We have taken the mean of the 100 highest axial coordinates reconstructed for the tracer at different gas velocities. Knowing the bed expansion, the overall gas holdup can be calculated considering the liquid–solid volume at rest. Fig. 14 shows the influence of gas velocity on gas holdup calculated in this way (closed symbols) both for the foaming and non-foaming systems. For comparison, chordal gas holdups determined by gamma densitometry at three column heights near the axial center have also been included in the figure. Reasonably good agreement has been found between the two independent experimental procedures, particularly for the non-foaming system.

As observed in the profiles, gas holdups in foaming systems are larger than in non-foaming systems at the same gas velocity, in agreement with results reported in the literature [2,30,31]. From the gas holdup *vs.* gas velocity curve, the gas velocity leading to a change in flow regime can be estimated from the trend break. The gas velocity leading to a flow transition is indicated in Fig. 13 for both systems. Flow transition is also affected by the presence of foam, being shifted towards higher gas velocity values.

4. Conclusions

The motion of a solid tracer representing an immobilized or aggregated cell biocatalyst is examined, to get characteristic features of the particles motion within foaming and comparable non-foaming gas–liquid system. Results indicate that:

- The axial and radial solid velocities close to the wall are affected by the presence of foam, likely arising from a hindrance effect of the foam that prevents the solid to remain in the wall vicinity. An inwards flow is observed in foaming systems, leading to more negative radial velocities and less definite negative axial velocities in the region. The rise velocities are slightly higher in the column center for the non-foaming system.
- There is considerable damping of the turbulence intensity distribution in foaming systems, reducing the highest and mean values to less than half in the overall TKE distributions. The largest decrease is observed in the disengagement region, mainly arising from inhibited bubble bursts. The influence of the gas velocity on the TKE is considerably reduced in the upper region of the column, particularly under the heterogeneous flow regime. In the entrance region, differences between foaming and non-foaming systems are small, indicating that the turbulence intensity is related mostly to the gas jets in the injection.
- The axial and radial dispersion coefficients are smaller in the foaming systems compared to results obtained for comparable non-foaming conditions. Differences are enhanced in the heterogeneous flow regime.
- Solid mixing times are similar for both systems. There is an axial location, around two column diameters above the gas injection, from which the time required to attain the asymptotic solid distribution is the minimum.
- The gas holdup is increased in foaming systems and the flow transition is shifted towards higher gas velocities.

References

[1] J.J. Chalmers, Mixing, aeration and cell damage, 30+ years later: What we learned, how it affected the cell culture industry and what we would like to know more about, *Curr. Opin. Chem. Eng.* 10 (2015) 94–102.
[2] M.P. Dudukovic, Frontiers in reactor engineering, *Science* 325 (2009) 698–701.
[3] M.-L. Collignon, A. Delafosse, M. Crine, D. Toye, Axial impeller selection for anchorage dependent animal cell culture in stirred bioreactors: Methodology based on the impeller comparison at just-suspended speed of rotation, *Chem. Eng. Sci.* 65 (2010) 5929–5941.
[4] C. Haringa, W. Tang, A.T. Deshmukh, J. Xia, M. Reuss, J.J. Heijnen, R.F. Mudde, H.J. Noorman, Euler-Lagrange computational fluid dynamics for (bio)reactor scale down: An analysis of organism lifelines, *Eng. Life Sci.* 16 (2016) 652–663.
[5] R.M. Shenkman, R. Godoy-Silva, K.K. Papas, J.J. Chalmers, Effects of energy dissipation rate on islets of langerhans: Implications for isolation and transplantation, *Biotechnol. Bioeng.* 103 (2009) 413–423.
[6] A. Shaikh, M. Al-Dahhan, Scale-up of bubble column reactors: A review of current state-of-the-art, *Ind. Eng. Chem. Res.* 52 (2013) 8091–8108.
[7] A. Cruz, L. Couto, S. Esplugas, C. Sans, Study of the contribution of homogeneous catalysis on heterogeneous Fe(III)/alginate mediated photo-Fenton process, *Chem. Eng. J.* 318 (2017) 272–280.
[8] K. Guo, T. Wang, G. Yang, J. Wang, Distinctly different bubble behaviors in a bubble column with pure liquids and alcohol solutions, *J. Chem. Technol. Biotechnol.* 92 (2017) 432–441.
[9] G. Besagni, F. Inzoli, G. de Guido, L.A. Pellegrini, Experimental investigation on the influence of ethanol on bubble column hydrodynamics, *Chem. Eng. Res. Des.* 112 (2016) 1–15.
[10] M. Moo-Young, M. Butler, C. Webb, A. Moreira, B. Grodzinski, Z.F. Cui, S. Agathos, Comprehensive Biotechnology, 2nd ed. Elsevier, 2011.
[11] S. Laorrattanasak, W. Rongsayamanont, N. Khondee, N. Paorach, S. Soonglerdsongpha, O. Pinyakong, E. Luepromchai, Production and application of *Gordonia westfalica* GY40 biosurfactant for remediation of fuel oil spill, *Water Air Soil Pollut.* (2016) 227–325.
[12] S. Yao, S. Zhao, Z. Lu, Y. Gao, F. Lv, X. Bie, Control of agitation and aeration rates in the production of surfactin in foam overflowing fed-batch culture with industrial fermentation, *Rev. Argent. Microbiol.* 47 (2015) 344–349.
[13] V. Rangarajan, R. Sen, An inexpensive strategy for facilitated recovery of metals and fermentation products by foam fractionation process, *Colloids Surf. B* 104 (2013) 99–106.
[14] S. Chenikher, J.S. Guez, F. Coutte, M. Pekpe, P. Jacques, J.P. Cassar, Control of the specific growth rate of *Bacillus Subtilis* for the production of biosurfactant lipopeptides in bioreactors with foam overflow, *Process Biochem.* 45 (2010) 1800–1807.

[15] J.S. Guez, S. Chenikher, J.P. Cassar, P. Jacques, Setting up and modelling of overflowing fed-batch cultures of *Bacillus Subtilis* for the production and continuous removal of lipopeptides, *J. Biotechnol.* 131 (2007) 67–75.
[16] M. Vesvikar, M.H. Al-Dahhan, Hydrodynamics investigation of laboratory-scale internal gas-lift loop anaerobic digester using non-invasive CAPRT technique, *Biomass Bioenergy* 84 (2016) 98–106.
[17] G. Salierno, M. Maestri, S. Piovano, M. Cassanello, M.A. Cardona, D. Hojman, H. Somacal, Calcium alginate beads motion in a foaming three-phase bubble column, *Chem. Eng. J.* 324 (2017) 358–369.
[18] B. Lee, P. Ravindra, E. Chan, Size and shape of calcium alginate beads produced by extrusion dripping, *Chem. Eng. Technol.* 36 (2013) 1627–1642.
[19] N.E. Holden, Neutron Capture Cross Section Standards for BNL 325, 4th edition National Nuclear Data Center. Brookhaven National Laboratory, 1981.
[20] G. Salierno, Caracterización de equipos y medios multifásicos con métodos que emplean fuentes radiactivas PhD Thesis, Universidad de Buenos Aires, Argentina, 2016 (http://digital.bl.fcen.uba.ar/Download/Tesis/Tesis_5951_Salierno.pdf).
[21] J. Chaouki, F. Larachi, M.P. Dudukovic (Eds.), Non-Invasive Monitoring of Multiphase Flows, Elsevier, Amsterdam, 1997.
[22] F. Larachi, M. Cassanello, J. Chaouki, C. Guy, Flow structure of the solids in a 3-D gas-liquid-solid fluidized bed, *AICHE J.* 42 (1996) 2439–2452.
[23] S. Degaleesan, M.P. Dudukovic, Y. Pan, Experimental study of gas-induced liquid-flow structures in bubble columns, *AICHE J.* 47 (2001) 1913–1931.
[24] S.S. Barretto, F. Michoux, K. Hellgardt, P.J. Nixon, Pneumatic hydrodynamics influence transplastomic protein yields and biological responses during in vitro shoot regeneration of *Nicotiana tabacum callus*: Implications for bioprocess routes to plant-made biopharmaceuticals, *Biochem. Eng. J.* 117 ((2017) 73–81.
[25] Y. Liu, Z.-J. Wang, J.-Y. Xia, C. Haringa, Y.-P. Liu, J. Chu, Y.-P. Zhuang, S.-L. Zhanga, Application of Euler–Lagrange CFD for quantitative evaluating the effect of shear force on *Carthamus tinctorius L.* cell in a stirred tank bioreactor, *Biochem. Eng. J.* 114 (2016) 209–217.
[26] A. Braga, D.P. Mesquita, A.L. Amaral, E.C. Ferreira, I. Belo, Aroma production by *Yarrowia lipolytica* in airlift and stirred tank bioreactors: Differences in yeast metabolism and morphology, *Biochem. Eng. J.* 93 (2015) 55–62.
[27] C. Zhong, Y.-J. Yuan, Responses of *Taxus cuspidata* to hydrodynamics in bubble column bioreactors with different sparging nozzle sizes, *Biochem. Eng. J.* 45 (2009) 100–106.
[28] G. Salierno, M. Maestri, S. Piovano, M. Cassanello, M.A. Cardona, D. Hojman, H. Somacal, Discrete axial motion of a radioactive tracer reconstructed from the response of axially aligned detectors: Application to the analysis of a bubble column dynamics, *Chem. Eng. Sci.* 100 (2013) 402–412.
[29] A. Ben-Naim, Statistical Thermodynamics Based on Information, World Scientific Publishing Co. Pte. Ltd., Singapore, 2008.
[30] G. Besagni, F. Inzoli, The effect of liquid phase properties on bubble column fluid dynamics: Gas holdup, flow regime transition, bubble size distributions and shapes, interfacial areas and foaming phenomena, *Chem. Eng. Sci.* 170 (2017) 270–296.
[31] D. Rudkevitch, A. Macchi, Hydrodynamics of a high pressure three-phase fluidized bed subject to foaming, *Can. J. Chem. Eng.* 86 (2008) 293–301.